Soft Sponge Sensor for Multimodal Sensing and Distinguishing of Pressure, Strain, and Temperature

Li-Wei Lo,[†,§] Junyi Zhao,[†] Haochuan Wan,[†] Yong Wang,[†,‡] Shantanu Chakrabartty,[†,] and Chuan Wang[,†,§]*

[†] Department of Electrical & Systems Engineering, Washington University in St. Louis, St. Louis, Missouri 63130, United States

[§] Institute of Materials Science and Engineering, Washington University in St. Louis, St. Louis, Missouri 63130, United States

[‡] Department of Obstetrics & Gynecology, Washington University in St. Louis, St. Louis, Missouri 63130, United States

[*] Corresponding author: chuanwang@wustl.edu

ABSTRACT

Soft wearable sensors are essential components for applications such as motion tracking, human-machine interface, and soft robots. However, most of the reported sensors are either specifically designed to target an individual stimulus or capable of responding to multiple stimuli (*e.g.,* pressure and strain) but without the necessary selectivity to distinguish those stimuli. Here we report an elastomeric sponge-based sensor that can respond to and distinguish three different kinds of stimuli: pressure, strain, and temperature. The sensor utilizes a porous polydimethylsiloxane (PDMS) sponge fabricated from a sugar cube sacrificial template, which was subsequently coated with a poly(3,4-ethylenedioxythiophene) polystyrene sulfonate (PEDOT:PSS) conductive polymer through a low-cost dip-coating process. Responses to different types of stimuli can be

distinguished by simultaneously recording resistance and capacitance changes. Because pressure, tensile strain, and temperature change result in different trends in resistance and capacitance change, those stimuli can be clearly distinguished from each other by simultaneously measuring the resistance and capacitance of the sensor. We have also studied the effect of the pore size on the sensor performance and have found that the sponge sensor with smaller pores generally offers greater resistance change and better sensitivity. As a proof-of-concept, we have demonstrated the use of the porous sponge sensor on an artificial hand for object detection, gesture recognition, and temperature sensing applications.

KEYWORDS: multimodal sensor, porous PDMS, conductive polymer, wearable sensors, stretchable electronics

Figure for TOC

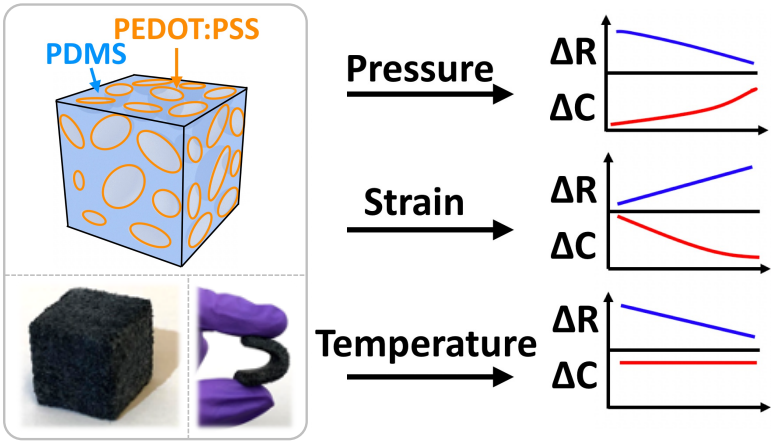

INTRODUCTION

The development of soft wearable electronic devices and sensors has attracted significant attention recently due to their wide range of applications in health monitoring,[1] body motion tracking,[2] deformable displays,[3] and many others. Unlike conventional electronics manufactured on rigid and brittle wafers, soft electronic devices and sensors attempt to match the mechanical properties of human skin,[4] and they offer desirable features such as elasticity that allows the device to be stretched and compressed while maintaining electrical performance and reliability. Stretchable pressure sensor,[5] strain sensor,[6] electrocardiogram (ECG) sensor,[7] and photoplethysmography sensor[8] integrated with stretchable electronic interconnects that can be stretched by up to several tens, or even hundreds of percent have all been demonstrated. Owing to their unique properties, these soft sensors can form intimate contact with the human skin to allow high precision signal recording and also provide great wearing comfort. As a result, they have been extensively studied for wearable health monitoring device applications.

Many of the soft wearable sensors reported in the literature are designed to target the detection of one specific physical or chemical signal. There are some resistive, capacitive, piezoelectric, or triboelectric sensors that are responsive to multiple different stimuli but the selectivity and how to determine what causes the measured response become significant challenges.[9–12] Take pressure sensor as an example, pressure sensing rubber,[13] capacitive pressure sensor based on a structured dielectric layer,[14] or polyvinylidene fluoride-based piezoelectric pressure sensor[15] are good for pressure detection but not particularly suitable for measuring longitudinal strain. On the other hand, strain sensors based on the metal nanoparticles[16,17] or conductive nanocomposite[18,19] are typically not very sensitive or even incapable of detecting pressure stimulus. For applications such as wearable health monitoring devices, soft robotics, and many others, it is often desirable to have multimodal sensor devices that are capable of responding to a variety of physical or chemical stimuli. In order to achieve multimodal sensing, one solution is to integrate multiple single-modality sensors into a single sensor device. One example is a planar-type sensor patch with integrated acceleration, temperature, and electrocardiogram sensors to monitor the human motion, skin temperature, and electrocardiogram signals simultaneously.[20] Another example is a device with a layer-by-layer sandwich structure with humidity, thermal, and pressure sensors stacked on top of each other to monitor various motion and daily life activities.[21] Nevertheless, integrating

multiple sensors into either planar-type or sandwiched structure and recording each electrical signal independently not only requires a more complex systems and read out circuits but also a more sophisticated fabrication processes and interconnects, which is not necessarily a preferred solution when low-cost sensors are needed.

Alternatively, a number of research groups have reported new device structures capable of detecting various mechanical stimuli and differentiate the stimuli in a single device by utilizing multiple sensing layers.[22,23] For example, sensors with sandwiched multilayer structure comprising polydimethylsiloxane (PDMS)/ single-walled carbon nanotube (SWNT) film/porous PDMS/PDMS spacers/SWNT-film/PDMS have been reported to detect and differentiate tensile strain due to the change in resistance within SWNTs film and normal pressure from the change in capacitance. In addition, the sensor can also harvest a variety of mechanical energy owing to the triboelectric effect between SWNT, porous PDMS, and the air gap created by PDMS spacers.[24] Sensors based on mechanical interlocking with metal-coated, high-aspect-ratio polyurethane acrylate nanofibres sandwiched between elastomer layers can also achieve pressure, shear, and torsion detection simultaneously and differentiate each stimulus by the magnitudes and frequencies of the corresponding signals.[25] Lastly, a multilayer sensor constructed with polytetrafluoroethylene film, copper sheets, silver nanowires film and a sponge-like graphene/polydimethylsiloxane composite has also been reported to perform pressure, temperature sensing, and material identification due to piezoresistive, thermoelectric, and triboelectric effects.[26]

Despite the significant progress on multimodal sensors described above, it is clear that many of the solutions still require fairly complex device structures and fabrication processes. Here, we report a multimodal sensor with a very simple single-layer device structure comprising a porous PDMS sponge coated with a conductive poly(3,4-ethylenedioxythiophene):polystyrene sulfonate (PEDOT:PSS) layer. The sensor can achieve pressure, strain, and temperature sensing and with the ability to distinguish the stimuli. To fabricate the porous PDMS sponge, a commercially available sugar cube was used as a sacrificial template, which can be subsequently leached in hot water. After the PDMS sponge was formed, it was thoroughly coated with a thin layer of a PEDOT:PSS conductive polymer through a low-cost dip-coating process. The ability to respond to three kinds of stimuli and with the selectivity to distinguish whether the response was caused

by pressure, strain, or temperature was achieved by simultaneously measuring both the resistance and capacitance changes and the different trends in their responses (*i.e.,* decrease in resistance and increase in capacitance under pressure; increase in resistance and decrease in capacitance under tensile strain; decrease in resistance and negligible change in capacitance under elevated temperature). The effect of micropore size on the mechanical properties and sensitivity of the sensor has also been studied. If resistance change is used as the calibration curve to quantify the stimuli, then the porous PEDOT:PSS/PDMS sponge sensor with a smaller pore size generally improves sensitivity. Due to the high sensitivity to pressure, strain, and temperature change, the porous PEDOT:PSS/PDMS sponge sensor could have various applications toward motion sensing and sensors for soft robots. As a proof-of-concept, we have demonstrated the use of the sensor on an artificial hand for object detection, gesture recognition, and temperature sensing applications.

RESULTS AND DISCUSSION

The porous PEDOT:PSS/PDMS sensor is capable of detecting and distinguishing pressure, strain, and temperature stimuli. The concept of the sensor's response curves to various types of stimuli are schematically illustrated in Figure 1a. When external pressure is applied normal to the top surface of the sensor, the electrical properties of the sensor change. The sensor's electrical resistance decreases due to the increase of contacts between the PEDOT:PSS thin film coated on the porous PDMS sponge, which results in more paths for electrical conduction. In the meantime, the compression of the micropores within the PDMS results in an increase in capacitance because the volume percentage of air in the sensor decreases and the dielectric constant of PDMS (ε_{PDMS} = 2.77) is greater than the air (ε_{air} = 1.0006).[27,28] In contrast, when a tensile strain is applied along the longitudinal direction of the sensor, the resistance increases due to the elongation of the sensor, which disrupted the conductive PEDOT:PSS thin film, and the capacitance decreases due to the increase in distance of the sponge between the electrodes. Lastly, as the temperature rises, the increase in thermal energy aids the carrier transport and charge hopping between the PEDOT grains, resulting in a decrease in resistance, whereas the capacitance remains almost unchanged. Therefore, by simultaneously measuring both the electrical resistance and capacitance, the different trends in resistance and capacitance change will allow us to differentiate whether the detected stimulus is from pressure, strain, or temperature. A more detailed study about the sensing mechanism will be discussed in the following paragraphs.

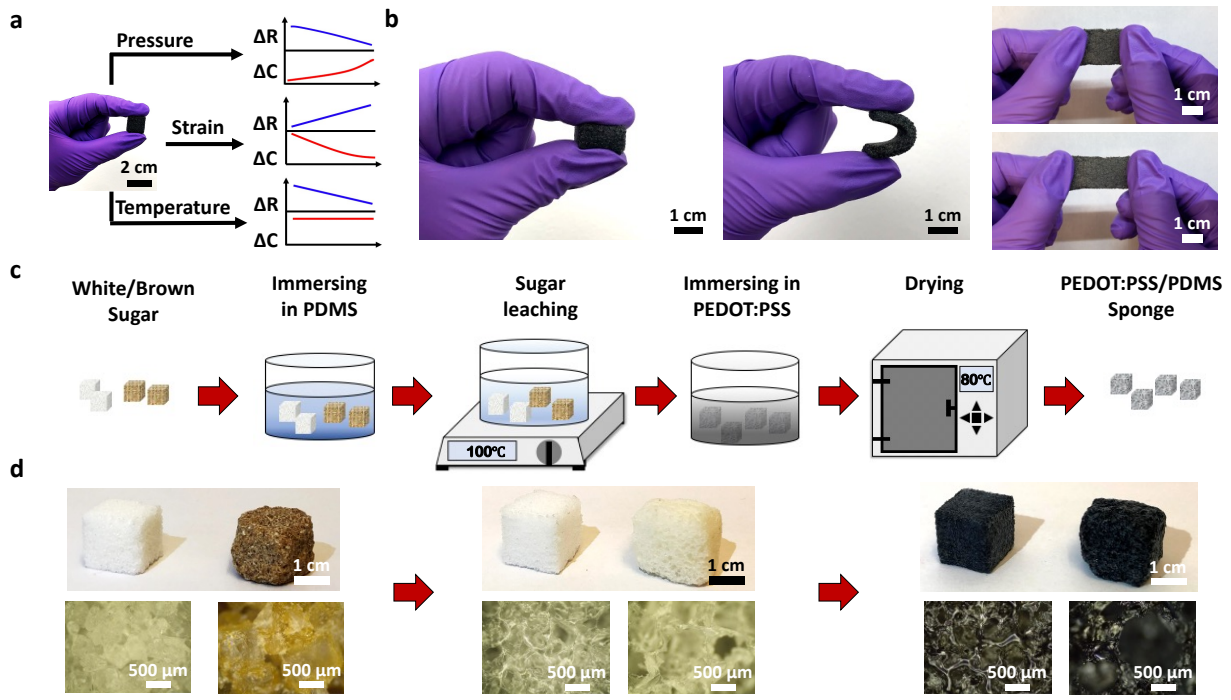

Figure 1. Multimodal sensor based on porous PEDOT:PSS/PDMS sponge. (a) Schematics illustrating the different trends in resistance and capacitance change caused by different physical stimuli. (b) Photos showing the compressibility, bendability and stretchability of the porous PEDOT:PSS/PDMS sponge sensor. (c) Schematics illustrating the fabrication steps of the porous PEDOT:PSS/PDMS sponge sensor. (d) Photos and optical micrographs showing the white and brown sugar cubes used as templates, the corresponding PDMS and PEDOT:PSS/PDMS sponges after each fabrication step.

The compressibility, bendability, and stretchability of the porous PEDOT:PSS/PDMS sensor are shown in Figure 1b. The shape of the sensor would fully recover after the external stimuli were released. The fabrication processes of the porous PEDOT:PSS/PDMS sensor are schematically illustrated in Figure 1c. More details about the fabrication steps and the formulation of conductive PEDOT:PSS ink can be found in the Method Section. In brief, the processes start from commercially available sugar cubes immersed in PDMS liquid, followed by the solidification of PDMS. The sugar/PDMS cubes are then placed in hot water to leach the sugar particles, which results in porous PDMS sponges. Due to the hydrophobicity of PDMS, the PDMS sponges were pretreated with oxygen plasma to improve the wetting of the PEDOT:PSS ink. After the oxygen plasma treatment, the porous PDMS sponges were first immersed in PEDOT:PSS solution and subsequently placed in an air oven to anneal the PEDOT:PSS thin film. After the above processes,

conductive PEDOT:PSS thin film was successfully coated onto the porous PDMS. Both optical photos and optical micrographs of the sugar cubes, porous PDMS sponges, and porous PEDOT:PSS/PDMS sponges (from left to right) are shown in Figure 1d. As shown in the left images of Figure 1d, both brown and white sugar cubes were used in this study, with brown sugar exhibiting a larger sugar particle size (700 – 1000 μm) than the white sugar (300 – 500 μm). The center images are the porous PDMS sponges formed after sugar leaching. The micropores inside the porous PDMS sponge made with brown sugar is larger than the ones inside the sponge made with white sugar, which is as expected based on the original sugar particle size. The use of different sugar templates allows us to study the effect of micropore size on the sensor response. Lastly, after the PEDOT:PSS coating process, the white color of the porous PDMS sponge turns into black color porous PEDOT:PSS/PDMS sponge, as shown in the images on the right-hand side of Figure 1d.

We have performed the microstructure and the element composition analysis of the porous PDMS sponge and the porous PEDOT:PSS/PDMS sponge by scanning electron microscopy (SEM) and the energy-dispersive X-ray spectroscopy (EDX). The structural formula of PDMS and PEDOT:PSS shown in Supporting Information Figure S1 suggests the element content of sulfur is present in PEDOT:PSS but not in PDMS. From the EDX analysis results of porous PDMS sponge shown in Figures 2a and 2b, carbon, oxygen, and silicon elements can be identified. In contrast, from the porous PEDOT:PSS/PDMS sponge, in addition to the three elements above, sulfur can also be found as shown in Figure 2c and 2d, which confirms that the PEDOT:PSS thin film has indeed been coated onto the inner surface of the PDMS sponge. One thing to note is that the small peak at around 1.041 keV ($K_\alpha = 1.041$) in Figure 2d is confirmed to be the impurity of sodium content from the glassware. More detailed information is presented in Figure S2 of the Supporting Information.

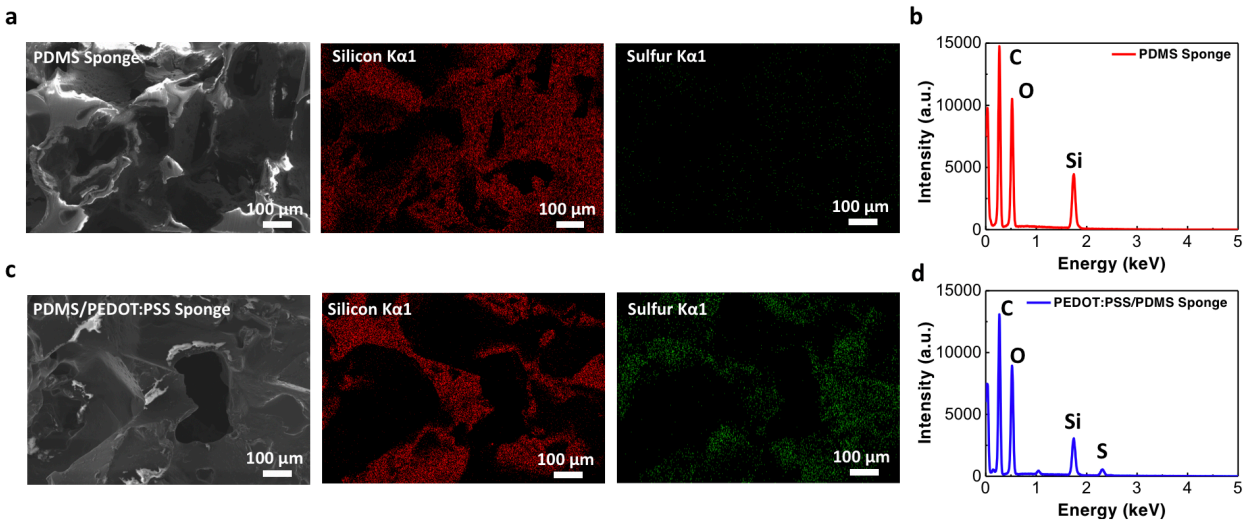

Figure 2. SEM and EDX analysis of the multimodal sponge sensor. (a) SEM and the corresponding EDX images of the PDMS sponge. (b) EDX spectrum of the PDMS sponge. (c) SEM and the corresponding EDX images of the PEDOT:PSS/PDMS sponge. (d) EDX spectrum of the PEDOT:PSS/PDMS sponge.

In this work, we used two types of sugar templates (white sugar and brown sugar) to fabricate the porous PEDOT:PSS/PDMS sensor to study and compare the effect of micropore size and porosity on the device sensitivity under compressive and tensile strain stimuli. As discussed in Figure 1d, the samples fabricated using white sugar cubes tend to have smaller micropore sizes and lower porosity than those fabricated using brown sugar. Details about the porosity calculation can be found in Supporting Information Table S1. As will be discussed below, both the pore size and porosity have a significant impact on the sensor's sensitivity and performance. Figure 3a shows the sensor response curve ($\Delta R/R_0$ *vs.* compressive strain) of the porous PEDOT:PSS/PDMS sensor when the device is being compressed to up to 70% strain. From the figure, one can see that the resistance of the sensor decreases with increasing compression strain. For example, under 20% compressive strain, the relative change in resistance of the sensors made from the white sugar and brown sugar are -13% and -5%, respectively. As the compressive strain increases to 70%, the relative change in resistance increases to -61% and -45% for sensors made from white and brown sugar, respectively. The mechanism of the decrease in resistance under compressive strain (*i.e.,* pressure applied normal to the top surface) can be attributed to the increase in the overlapping area of the PEDOT:PSS thin film coated on the inner surface of the porous PDMS sponge. When pressure is applied to the sensor, the micropores gradually close, and the conductive PEDOT:PSS thin film on the inner surface of the pores forms temporary contacts with each other, resulting in a

more conductive network. Once the pressure is released, the micropores return to their initial morphology, which causes the resistance to also return to the initial value. Furthermore, Figure 3a also shows that the sensor made from the white sugar cubes exhibits a more significant amount of change in resistance (*i.e.,* better sensitivity) than the sensor made from the brown sugar cubes. As indicated in Figure 1d, because the size of the micropores in the PDMS sponge made with white sugar cubes are smaller than the one made from brown sugar cubes, the smaller pore size results in a greater increase in conductive paths formed in PEDOT:PSS under the same amount of compressive strain. As a result, the sensor made from the white sugar cube exhibits a greater amount of change in resistance.

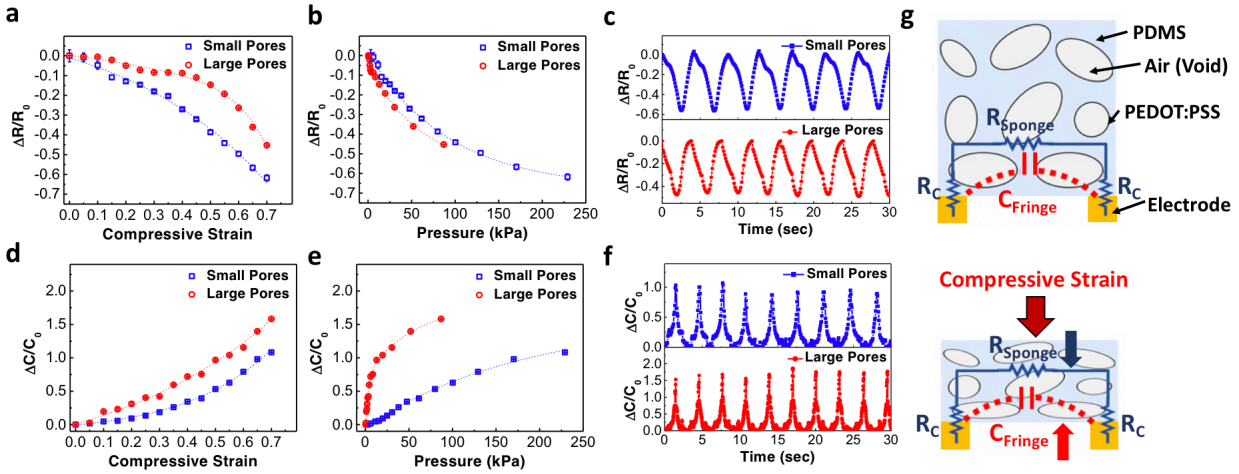

Figure 3. Electrical characterization of the porous PEDOT:PSS/PDMS sensor in response to compressive strain and pressure. (a) Relative change in resistance plotted as a function of compressive strain. Dotted lines: fitting curves. (b) Relative change in resistance plotted as a function of pressure. Dotted lines: fitting curves. (c) Dynamic response in resistance of the porous PEDOT:PSS/PDMS sensor when it was repeatedly compressed to a strain of 70% and released. (d) Relative change in capacitance plotted as a function of compressive strain. Dotted lines: fitting curves. (e) Relative change in capacitance plotted as a function of pressure. Dotted lines: fitting curves. (f) Dynamic response in capacitance of the porous PEDOT:PSS/PDMS sensor when it was repeatedly compressed to a strain of 70% and released. (g) Schematic illustration of the porous PEDOT:PSS/PDMS sponge sensor showing the increase in fringe capacitance and decrease in electrical resistance under compressive strain.

We have also measured the precise pressure applied onto the porous PEDOT:PSS/PDMS sensor under various amount of compressive strain using a commercially available force sensor (FSR 402 Interlink Electronics, Inc.). The sensing response as a function of pressure derived from Figure 3a

is plotted in Figure 3b. More details about the electro-mechanical setup can be found in the Methods section. From Figure 3b, one can see that the sensor made from the brown sugar cubes exhibits a slightly greater response when compared to the sensor made from white sugar cubes under the same amount of pressure. This is because the mechanical properties of the PDMS sponge also have a great impact on the sensor performance. Because the PEDOT:PSS/PDMS sponge sensor made from brown sugar has greater porosity (Table S1), it is softer than the sensor made from white sugar (compressive stress-strain curve shown in Supporting Information Figure S3), and therefore experiences higher compressive strain and larger deformation of the micropores under the same amount of pressure. Moreover, the sensor made from the brown sugar cubes can only be compressed up to 86 kPa, whereas the sensor made from white sugar can go up to 229 kPa at 70% of compressive strain. The dynamic response of the porous PEDOT:PSS/PDMS sensor has also been studied, and the results are presented in Figure 3c. The sensors were repeatedly compressed to a strain of 70% and then released to a relaxed state. The results show that the resistance decreases when the sensor is compressed and returns to the initial value after the pressure is released during each loading-unloading cycle, confirming the good repeatability of the sensor response.

The electrical capacitance of the sensor is also responsive to the compressive strain. Figure 3d shows the relative change in capacitance plotted as a function of compressive strain ($\Delta C/C_0$ *vs.* compressive strain), and Figure 3e shows the relative change in capacitance plotted as a function of pressure ($\Delta C/C_0$ *vs.* pressure). When pressure is applied, the capacitance of the sponge sensor increases due to an increase in its effective dielectric constant. More specifically, when a sponge sensor is in its relaxed state, the fringing capacitance is composed of the capacitance of the PDMS sponge and the air within the micropores. When the sensor gets compressed, the air is displaced, and a larger percentage of the volume is now composed of PDMS, which has a much greater permittivity than air (2.77 for PDMS *vs.* 1.00061 for air), resulting in an increase in the device capacitance. In terms of the relation between the pore size on the capacitance change, the relative change in capacitance is greater for the sample with a larger micropore size and higher porosity (sensor made from the brown sugar) both under the same compressive strain (Figure 3d) and pressure (Figure 3e). Similarly, the capacitance change in the porous PEDOT:PSS/PDMS sponge sensor also shows great repeatability, as can be seen from the dynamic response measurements in

Figure 3f. In summary, the mechanisms of the sensor response under compression discussed above are schematically illustrated in Figure 3g.

In addition to responding to compressive strain and pressure, the porous PEDOT:PSS/PDMS sensor can also respond well to tensile strain. Figure 4a shows the sensor response curve ($\Delta R/R_0$ *vs.* tensile strain) of the porous PEDOT:PSS/PDMS sponge when stretched to a strain of 30%. As the tensile strain increases, the porous PEDOT:PSS/PDMS sensors made from both white and brown sugar show an increase in resistance due to the disruption of PEDOT:PSS thin film. Similar to its response to pressure, the pore size of the sensor also affects its sensitivity and the response to the tensile strain. From the current-voltage curves measured from the porous PEDOT:PSS/PDMS sensors in their relaxed state (Supporting Information Figure S4 and Table S2), one can find that the resistance (R_0) of the sensor made from white sugar cube (smaller pore size) is greater than the sensor made from the brown sugar cube (larger pore size). The higher resistance in the relaxed state from the porous PEDOT:PSS/PDMS sensor with smaller pores suggests that the coating layer thickness and the content of conductive PEDOT:PSS on the PDMS sponge with smaller pores may be less than the one with larger pores. The smaller pore size also results in a more significant increase in resistance under the same amount of tensile strain. For example, when the sensor is stretched to a strain of 10%, the sensor made from the white sugar cubes exhibits a resistance increase of 21.4% compared to 14.0% for the sensor made from brown sugar cubes. As the tensile strain increases to 30%, the sensor made from the white sugar cubes exhibits a resistance increase of 150% compared to 42% for the sensor made from brown sugar cubes. The greater response and better sensitivity from the sponge sensor with smaller pore size can be attributed to the smaller thickness of PEDOT:PSS coating on the sponge, which makes the PEDOT:PSS conductive pathway in the sensor made from white sugar cubes more easily to be disrupted upon longitudinal stretch leading to a greater change in resistance under the same amount of tensile strain. The dynamic response of the porous PEDOT:PSS/PDMS sensor under tensile strain is also measured and shown in Figure 4b. Both sensors were repeatedly stretched to a strain of 30% and released, and the sensor response ($\Delta R/R_0$) remained stable after each stretching-releasing cycle.

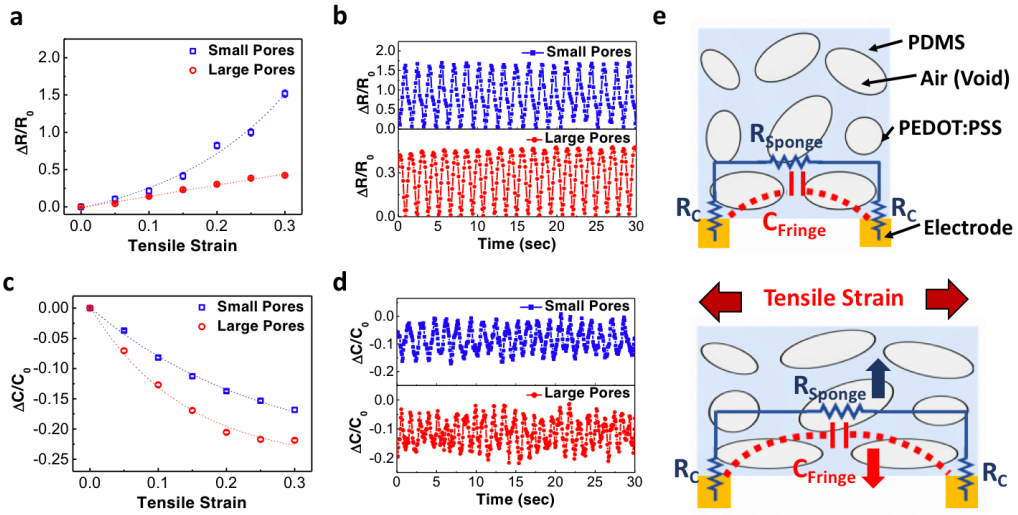

Figure 4. Electrical characterization of the porous PEDOT:PSS/PDMS sensor in response to tensile strain. (a) Relative change in resistance plotted as a function of tensile strain. Dotted lines: fitting curves. (b) Dynamic response in resistance of the porous PEDOT:PSS/PDMS sensor when it was repeatedly stretched to a strain of 30% and released. (c) Relative change in capacitance plotted as a function of tensile strain. Dotted lines: fitting curves. (d) Dynamic response in capacitance of the porous PEDOT:PSS/PDMS sensor when it was repeatedly stretched to a strain of 30% and released. (e) Schematic illustration of the porous PEDOT:PSS/PDMS sponge sensor showing the decrease in fringe capacitance and increase in electrical resistance under tensile strain.

Figure 4c shows the capacitance change of the porous PEDOT:PSS/PDMS sponge sensor ($\Delta C/C_0$ *vs.* tensile strain) when stretching to a strain of 30%. The sensor exhibits a decrease in capacitance under tensile strain due to an increase in distance between two contact electrodes and a reduction in effective dielectric constant when the sponge is stretched. Comparing the sensors made from the white sugar cubes and the brown sugar cubes, the latter exhibits a greater change in capacitance under the same amount of tensile strain, which arises from the larger micropore size and the higher porosity causing a greater change in air volume and a more significant decrease in dielectric constant. In summary, for both pressure and tensile strain stimuli, smaller pore size results in a greater change in resistance and less change in capacitance. For dynamic response, similar to the resistance change presented in Figure 4b, the capacitance change of the porous PEDOT:PSS/PDMS sensor (Figure 4d) also remains stable and shows no noticeable degradation under cyclic stretch tests to a strain of 30%. The long-term stability test results with up to 1000 cycles can be found in Supporting Information Figure S5 and S6. Figure 4e schematically illustrates the mechanisms of the sensor response under tensile strain.

Because PEDOT:PSS is a well-known temperature-sensitive conductive polymer, [29–32] it can also be used for temperature sensing applications. For the experiments below, porous sensors with smaller pore sizes were used. The electrical conductivity depends on the charge transport along the conductive PEDOT grains and the charge hopping between the PEDOT and PSS grains. As the temperature increases, the increased thermal energy makes it more likely for charge carriers to overcome the potential barriers and hop between the adjacent grains, which results in a decrease in the resistance of the film. Figures 5a and b show the resistance and capacitance change of the porous PEDOT:PSS/PDMS sponge sensor measured at various temperatures. The resistance decreases linearly with increasing temperature due to the enhancement of charge transport discussed above, and the results are also consistent with previously reported work.[33] In terms of the capacitance, the measured change was only -2.0% when the sample was heated from room temperature to 80 °C, which was much smaller compared to the changes measured under compressive or tensile strain. The slight decrease in capacitance under heating could be attributed to the thermal expansion of the porous PDMS due to its high thermal expansion coefficient, which would lead to a reduction in capacitance similar to the tensile strain case analyzed above. We tested the sensor under repeated heating and cooling cycles from between 20 and 80 °C and confirmed that its response was repeatable. Additional data with more heating/cooling cycles can be found in Supporting Information Figure S7.

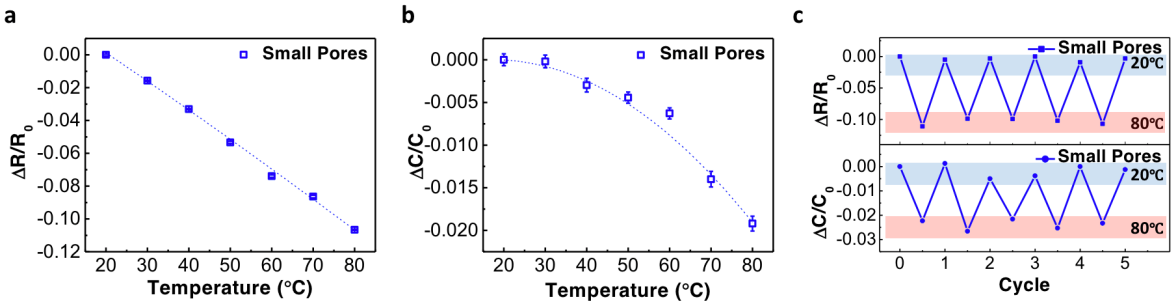

Figure 5. Electrical characterization of the porous PEDOT:PSS/PDMS sensor in response to temperature change. (a) Relative change in resistance plotted as a function of temperature. Dotted line: fitting curve. (b) Relative change in capacitance plotted as a function of temperature. Dotted line: fitting curve. (c) Dynamic response of the porous PEDOT:PSS/PDMS sensor under cyclic heating and colling between 20 °C and 80 °C.

Because the resistance and capacitance change in the porous PEDOT:PSS/PDMS sensor exhibit different trends for different stimuli, selectivity can be achieved by simultaneously measuring the device resistance and capacitance. The ability to differential pressure, strain, and temperature could enable various applications in smart wearables. In Figure 6, we have shown that the above porous PEDOT:PSS/PDMS sensors can be attached to different positions on an artificial hand to demonstrate object detection, gesture recognition, and temperature sensing applications. For example, if a resistance decrease and a capacitance increase are measured from the sensor, it can be inferred as a pressure stimulus applied on its surface. In contrast, when the resistance increases and the capacitance decreases, it means the sensor is being stretched. Lastly, when the resistance decreases but with no noticeable change in capacitance, it could be interpreted as increasing temperature. In Figure 6a, five sponge sensors were attached to the fingertips to detect the pressure exerted on the fingertip when the hand was grabbing an object. The resistance and capacitance data clearly show that when the hand was holding an object, only the sensors on figures that were in contact with the object showed decrease in electrical resistance and an increase in capacitance. By comparing the resistance and capacitance change with the response curve in Figures 3b and e, it is possible to determine the precise pressure on each fingertip using the fitting equations in the supporting information Table S3. In Figure 6b, the sensors were attached to the finger joints to measure the bending angle of the joints to determine the hand gestures. When the palm was fully open, there was no bending in any of the sensors and thus no change in resistance and capacitance. When the figures were bent, the sponge sensors were stretched, and the tensile strain resulted in an increase in resistance and a decrease in capacitance. The resistance and capacitance values could be used to determine the strain applied and the precise bending angle of each finger based on the data in Figure 4. Lastly, the porous PEDOT:PSS/PDMS sensor attached to the fingertips can also be used to detect the temperature change. As shown in Figure 6c, the artificial hand was placed on a hot plate heated to 20, 50, and 80 °C, respectively. As expected, the electrical data shows that the resistance decreases monotonically under elevated temperatures while the capacitance remains almost unchanged.

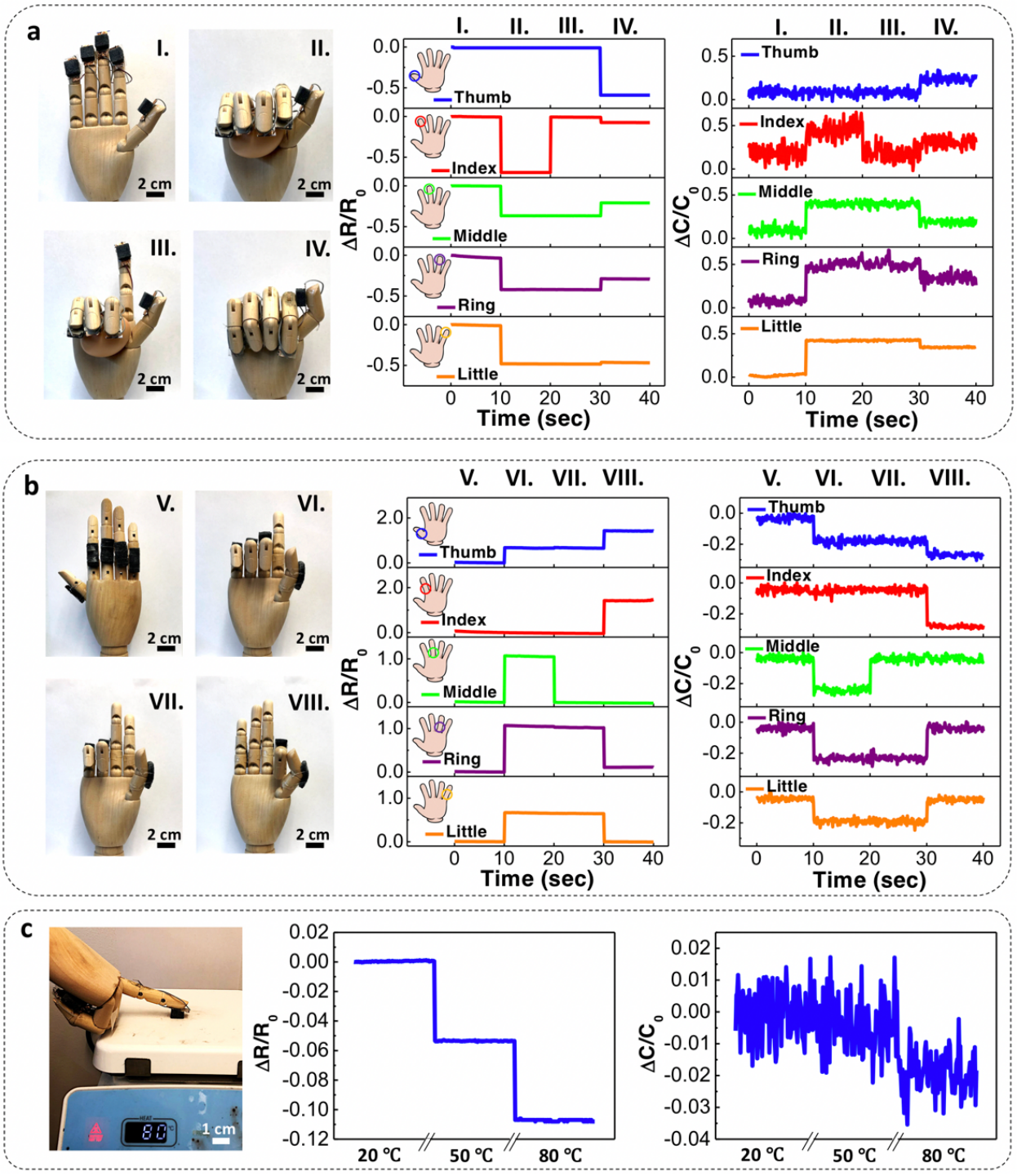

Figure 6. Application of the multimodal sponge sensor for object detection, gesture recognition, and temperature sensing. (a) Porous PEDOT:PSS/PDMS sensors were attached to the five fingertips of an artificial hand for pressure sensing application. Various fingers were brought into contact with the object in I, II, III, and IV, and responses can be measured in the corresponding sensors, which indicate the detection of contacts between the fingertips and the object. (b) Porous PEDOT:PSS/PDMS sensors were attached to the finger joints of an artificial

hand for gesture detection application. The five different fingers were bent to various amount in V, VI, VII, and VIII, and the correct responses can be measured in the corresponding sensors, allowing the gesture of the hand to be detected. (c) Porous PEDOT:PSS/PDMS sensor attached to the fingertip was brought into contact with a hot plate. The resistance change in the sensor allows the surface temperature to be measured.

CONCLUSION

In summary, we have achieved a soft, lightweight, and high sensitivity sponge sensor based on porous PDMS coated with a thin layer of PEDOT:PSS. The sensor can respond to and distinguish three different types of stimuli (pressure, strain, and temperature) through the changing resistance and capacitance. The mechanism of the sensor's response to different stimuli and the effect of the pore size on the sensor performance have been systematically studied. With its stretchability, sensitivity, and multimodality sensing capability, we have further demonstrated its application in pressure sensing, temperature sensing, object detection, and gesture recognition. The sensor developed in this work may lead to low-cost wearables for motion tracking and soft robotics applications.

METHODS

Materials

Polydimethylsiloxane (Sylgard 184) was purchased from Dow Corning. White sugar cube was purchased from C&H. Brown sugar cube was purchase from La Perruche. Poly(3,4-ethylenedioxythiophene)-poly(styrenesulfonate) (1.3 wt % dispersion in H_2O, conductive grade) and ethylene glycol (EG) (anhydrous, 99.8%) were purchased from Sigma-Aldrich. The silver conductive epoxy was purchase from MG Chemicals.

Preparation of the Porous PDMS Template

The PDMS was prepared by mixing the PDMS prepolymer with a curing agent with a mixing ratio of 10:1 w/w, and then a vacuum desiccator was used to remove the bubbles from the PDMS liquid. The sugar cubes 1.5 (W) x 1.5 (L) x 1.5 cm (H) were then dipped into the PDMS liquid for 2 h to let the pores inside the cubes be filled with PDMS liquid. After that, the sugar cubes filled with PDMS were cured in an oven for 3 h at 80 °C. The cubes were then placed in a hot water bath for 1 h at 100 °C to allow the sugar to be dissolved, leaving behind the PDMS sponge.

Preparation of the Porous PEDOT:PSS/PDMS Sensor

The porous PDMS sponge was cut into a size of 1.5 (W) x 1.5 (L) x 0.75 cm (H). To aid the wetting, the PEDOT:PSS ink on the hydrophobic PDMS surface, the porous PDMS sample was pretreated by oxygen plasma (Plasma Etch PE25) at 60 W for 30 s on both the top and bottom sides that are 1.5 (W) x 1.5 cm (L). 5 wt % ethylene glycol was added into the PEDOT:PSS solution and then stirred at room temperature for 1 h. The porous PDMS sponge was then dipped into the as-prepared PEDOT:PSS solution for 30 min. After that, the PEDOT:PSS-coated PDMS sponge was cured in the oven for 3 h at 80 °C.

Material Characterization of the Porous PEDOT:PSS/PDMS Sensor

The microstructure of the porous PDMS and porous PEDOT:PSS/PDMS was capture by both optical microscope (Olympus BX53M) and environmental scanning electron microscope (Thermofisher Quattro S ESEM). The element analysis was performed by environmental scanning electron microscope equipped with an energy dispersive X-ray spectrometer (Oxford AZtec).

Electrical Characterization of Porous PEDOT:PSS/PDMS Sensor

Silver conductive epoxy was applied at the bottom surface of the sensor to make electrical contacts between the sensor and the measurement instruments. The size of the silver conductive epoxy is 1.5 (W) x 0.1 cm (L). The porous PEDOT:PSS/PDMS sponge sensor was then placed on a

modified syringe pump with a 3D-printed loading platform for pressure measurement. A commercial force sensor (FSR 402, Interlink Electronics, Inc.) was attached to the bottom of the loading platform as a reference sensor that measures the actual pressure applied to the sensor. For the tensile strain testing, a modified syringe pump was used with the porous PEDOT:PSS/PDMS sensor clamped in between the moving stage. Temperature sensing experiments were performed on a heating plate. Both the resistance and capacitance measurements were recorded using a semiconductor device analyzer (Keysight B1500A). For the dynamic capacitance measurement, an evaluation board (EVAL-AD7746EB, Analog Devices, Inc.) was used to measure the continuous change of capacitance under pressure and tensile strain.

Conflict of Interest: The authors declare no competing financial interests.

Author Contributions:
L.L. and C.W. conceived the idea and designed the experiments. L.L. carried out the experiments including material and recipe development, sensor fabrication and characterization. J.Z. contributed to the PEDOT:PSS preparation. L.L., J.Z., H.W. Y.W. S.C. and C.W. contributed to the data analysis. L.L. and C.W. wrote the paper and all authors provided feedback and have given approval to the final version of the manuscript.

Acknowledgements:
This work was funded by Bill & Melinda Gates Foundation (INV-005417). The authors acknowledge the Washington University in St. Louis Institute of Materials Science and Engineering for the use of instruments and staff assistance.

Supporting Information Available: Chemical structures of PDMS and conducting polymer PEDOT:PSS (Figure S1); Origin of sodium content in the PEDOT:PSS/PDMS sponge sensor

(Figure S2); Mechanical characterization of the porous PEDOT:PSS/PDMS sponge sensor under compressive and tensile strain (Figure S3); Electrical characterization of the porous PEDOT:PSS/PDMS sponge sensor (Figure S4); Long-term stability of the sensor response to compressive strain (Figure S5); Long-term stability of the sensor response to tensile strain (Figure S6); Long-term stability of the sensor response to temperature change (Figure S7); Comparison of PDMS sponge porosity (Table S1); Resistance and capacitance values of the porous PEDOT:PSS/PDMS sponge sensor measured in relax state (Table S2); Equations for fitting the response curves to different stimuli (Table S3); Performance comparison of different types of multimodal sensor based on polymer and nanomaterial composites (Table S4). This material is available free of charge *via* the Internet at http://pubs.acs.org.

REFERNECES

(1) Yu, Y.; Nassar, J.; Xu, C.; Min, J.; Yang, Y.; Dai, A.; Doshi, R.; Huang, A.; Song, Y.; Gehlhar, R.; Ames, A. D.; Gao, W. Biofuel-Powered Soft Electronic Skin with Multiplexed and Wireless Sensing for Human-Machine Interfaces. *Sci. Robot.* **2020**, *5*, eaaz7946.

(2) Atalay, A.; Sanchez, V.; Atalay, O.; Vogt, D. M.; Haufe, F.; Wood, R. J.; Walsh, C. J. Batch Fabrication of Customizable Silicone-Textile Composite Capacitive Strain Sensors for Human Motion Tracking. *Adv. Mater. Technol.* **2017**, *2*, 1700136.

(3) Li, S.; Peele, B. N.; Larson, C. M.; Zhao, H.; Shepherd, R. F. A Stretchable Multicolor Display and Touch Interface Using Photopatterning and Transfer Printing. *Adv. Mater.* **2016**, *28*, 9770–9775.

(4) Yuk, H.; Lu, B.; Zhao, X. Hydrogel Bioelectronics. *Chem. Soc. Rev.* **2019**, *48*, 1642–1667.

(5) Choong, C. L.; Shim, M. B.; Lee, B. S.; Jeon, S.; Ko, D. S.; Kang, T. H.; Bae, J.; Lee, S. H.; Byun, K. E.; Im, J.; Jeong, Y. J.; Park, C. E.; Park, J. J.; Chung, U. I. Highly Stretchable Resistive Pressure Sensors Using a Conductive Elastomeric Composite on a Micropyramid Array. *Adv. Mater.* **2014**, *26*, 3451–3458.

(6) Cho, D.; Park, J.; Kim, J.; Kim, T.; Kim, J.; Park, I.; Jeon, S. Three-Dimensional Continuous Conductive Nanostructure for Highly Sensitive and Stretchable Strain Sensor. *ACS Appl. Mater. Interfaces* **2017**, *9*, 17369–17378.

(7) Jin, H.; Nayeem, M. O. G.; Lee, S.; Matsuhisa, N.; Inoue, D.; Yokota, T.; Hashizume, D.; Someya, T. Highly Durable Nanofiber-Reinforced Elastic Conductors for Skin-Tight Electronic Textiles. *ACS Nano* **2019**, *13*, 7905–7912.

(8) Lee, Y.; Chung, J. W.; Lee, G. H.; Kang, H.; Kim, J. Y.; Bae, C.; Yoo, H.; Jeong, S.; Cho, H.; Kang, S. G.; Jung, J. Y.; Lee, D. W.; Gam, S.; Hahm, S. G.; Kuzumoto, Y.; Kim, S. J.; Bao, Z.; Hong, Y.; Yun, Y.; Kim, S. Standalone Real-Time Health Monitoring Patch Based on a Stretchable Organic Optoelectronic System. *Sci. Adv.* **2021**, *7*, eabg9180.

(9) Ding, Y.; Xu, T.; Onyilagha, O.; Fong, H.; Zhu, Z. Recent Advances in Flexible and Wearable Pressure Sensors Based on Piezoresistive 3D Monolithic Conductive Sponges. *ACS Appl. Mater. Interfaces* **2019**, *11*, 6685–6704.

(10) Li, W.; Jin, X.; Zheng, Y.; Chang, X.; Wang, W.; Lin, T.; Zheng, F.; Onyilagha, O.; Zhu, Z. A Porous and Air Gap Elastomeric Dielectric Layer for Wearable Capacitive Pressure Sensor with High Sensitivity and a Wide Detection Range. *J. Mater. Chem. C* **2020**, *8*, 11468–11476.

(11) Li, W.; Jin, X.; Han, X.; Li, Y.; Wang, W.; Lin, T.; Zhu, Z. Synergy of Porous Structure and Microstructure in Piezoresistive Material for High-Performance and Flexible Pressure Sensors. *ACS Appl. Mater. Interfaces* **2021**, *13*, 19211–19220.

(12) Sun, P.; Wu, D.; Liu, C. High-Sensitivity Tactile Sensor Based on Ti2C-PDMS Sponge for Wireless Human-Computer Interaction. *Nanotechnology* **2021**, *32*, 295506.

(13) Jung, S.; Kim, J. H.; Kim, J.; Choi, S.; Lee, J.; Park, I.; Hyeon, T.; Kim, D. H. Reverse-Micelle-Induced Porous Pressure-Sensitive Rubber for Wearable Human-Machine Interfaces. *Adv. Mater.* **2014**, *26*, 4825–4830.

(14) Yang, J.; Luo, S.; Zhou, X.; Li, J.; Fu, J.; Yang, W.; Wei, D. Flexible, Tunable, and Ultrasensitive Capacitive Pressure Sensor with Microconformal Graphene Electrodes. *ACS Appl. Mater. Interfaces* **2019**, *11*, 14997–15006.

(15) Park, S. H.; Lee, H. B.; Yeon, S. M.; Park, J.; Lee, N. K. Flexible and Stretchable

Piezoelectric Sensor with Thickness-Tunable Configuration of Electrospun Nanofiber Mat and Elastomeric Substrates. *ACS Appl. Mater. Interfaces* **2016**, *8*, 24773–24781.

(16) Lee, J.; Kim, S.; Lee, J.; Yang, D.; Park, B. C.; Ryu, S.; Park, I. A Stretchable Strain Sensor Based on a Metal Nanoparticle Thin Film for Human Motion Detection. *Nanoscale* **2014**, *6*, 11932–11939.

(17) Zhang, S.; Cai, L.; Li, W.; Miao, J.; Wang, T.; Yeom, J.; Sepúlveda, N.; Wang, C. Fully Printed Silver-Nanoparticle-Based Strain Gauges with Record High Sensitivity. *Adv. Electron. Mater.* **2017**, *3*, 1700067.

(18) Qin, Y.; Peng, Q.; Ding, Y.; Lin, Z.; Wang, C.; Li, Y.; Xu, F.; Li, J.; Yuan, Y.; He, X.; Li, Y. Lightweight, Superelastic, and Mechanically Flexible Graphene/Polyimide Nanocomposite Foam for Strain Sensor Application. *ACS Nano* **2015**, *9*, 8933–8941.

(19) Amjadi, M.; Pichitpajongkit, A.; Lee, S.; Ryu, S.; Park, I. Highly Stretchable and Sensitive Strain Sensor Based on Silver Nanowire-Elastomer Nanocomposite. *ACS Nano* **2014**, *8*, 5154–5163.

(20) Yamamoto, D.; Nakata, S.; Kanao, K.; Arie, T.; Akita, S.; Takei, K. A Planar, Multisensing Wearable Health Monitoring Device Integrated with Acceleration, Temperature, and Electrocardiogram Sensors. *Adv. Mater. Technol.* **2017**, *2*, 1700057.

(21) Ho, D. H.; Sun, Q.; Kim, S. Y.; Han, J. T.; Kim, D. H.; Cho, J. H. Stretchable and Multimodal All Graphene Electronic Skin. *Adv. Mater.* **2016**, *28*, 2601–2608.

(22) Boutry, C. M.; Kaizawa, Y.; Schroeder, B. C.; Chortos, A.; Legrand, A.; Wang, Z.; Chang, J.; Fox, P.; Bao, Z. A Stretchable and Biodegradable Strain and Pressure Sensor for Orthopaedic Application. *Nat. Electron.* **2018**, *1*, 314–321.

(23) Peng, S.; Wu, S.; Yu, Y.; Xia, B.; Lovell, N. H.; Wang, C. H. Multimodal Capacitive and

Piezoresistive Sensor for Simultaneous Measurement of Multiple Forces. *ACS Appl. Mater. Interfaces* **2020**, *12*, 22179–22190.

(24) Kim, N.; Kee, S.; Lee, S. H.; Lee, B. H.; Kahng, Y. H.; Jo, Y. R.; Kim, B. J.; Lee, K. Highly Conductive PEDOT:PSS Nanofibrils Induced by Solution-Processed Crystallization. *Adv. Mater.* **2014**, *26*, 2268–2272.

(25) Pang, C.; Lee, G. Y.; Kim, T. Il; Kim, S. M.; Kim, H. N.; Ahn, S. H.; Suh, K. Y. A Flexible and Highly Sensitive Strain-Gauge Sensor Using Reversible Interlocking of Nanofibres. *Nat. Mater.* **2012**, *11*, 795–801.

(26) Wang, Y.; Wu, H.; Xu, L.; Zhang, H.; Yang, Y.; Wang, Z. L. Hierarchically Patterned Self-Powered Sensors for Multifunctional Tactile Sensing. *Sci. Adv.* **2020**, *6*, 1–10.

(27) Farcich, N. J.; Salonen, J.; Asbeck, P. M. Single-Length Method Used to Determine the Dielectric Constant of Polydimethylsiloxane. *IEEE Trans. Microw. Theory Tech.* **2008**, *56*, 2963–2971.

(28) Meyer, J.; Arnrich, B.; Schumm, J.; Troster, G. Design and Modeling of a Textile Pressure Sensor for Sitting Posture Classification. *IEEE Sens. J.* **2010**, *10*, 1391–1398.

(29) Ouyang, J.; Xu, Q.; Chu, C. W.; Yang, Y.; Li, G.; Shinar, J. On the Mechanism of Conductivity Enhancement in Poly(3,4- Ethylenedioxythiophene):Poly(Styrene Sulfonate) Film through Solvent Treatment. *Polymer.* **2004**, *45*, 8443.

(30) Vitoratos, E.; Sakkopoulos, S.; Dalas, E.; Paliatsas, N.; Karageorgopoulos, D.; Petraki, F.; Kennou, S.; Choulis, S. A. Thermal Degradation Mechanisms of PEDOT:PSS. *Org. Electron.* **2009**, *10*, 61–66.

(31) Zhou, J.; Anjum, D. H.; Chen, L.; Xu, X.; Ventura, I. A.; Jiang, L.; Lubineau, G. The Temperature-Dependent Microstructure of PEDOT/PSS Films: Insights from

Morphological, Mechanical and Electrical Analyses. *J. Mater. Chem. C* **2014**, *2*, 9903–9910.

(32) Pradhan, S.; Yadavalli, V. K. Photolithographically Printed Flexible Silk/PEDOT:PSS Temperature Sensors. *ACS Appl. Electron. Mater.* **2021**, *3*, 21–29.

(33) Wang, Y. F.; Sekine, T.; Takeda, Y.; Yokosawa, K.; Matsui, H.; Kumaki, D.; Shiba, T.; Nishikawa, T.; Tokito, S. Fully Printed PEDOT:PSS-Based Temperature Sensor with High Humidity Stability for Wireless Healthcare Monitoring. *Sci. Rep.* **2020**, *10*, 2467.

Soft Sponge Sensor for Multimodal Sensing and Distinguishing of Pressure, Strain, and Temperature

Li-Wei Lo,[†,§] Junyi Zhao,[†] Haochuan Wan,[†] Yong Wang,[†,‡] Shantanu Chakrabartty,[†,] and Chuan Wang[,†,§]*

[†] Department of Electrical & Systems Engineering, Washington University in St. Louis, St. Louis, Missouri 63130, United States

[§] Institute of Materials Science and Engineering, Washington University in St. Louis, St. Louis, Missouri 63130, United States

[‡] Department of Obstetrics & Gynecology, Washington University in St. Louis, St. Louis, Missouri 63130, United States

[*] Corresponding author: chuanwang@wustl.edu

Supporting information

S1. Chemical structures of PDMS and conducting polymer PEDOT:PSS

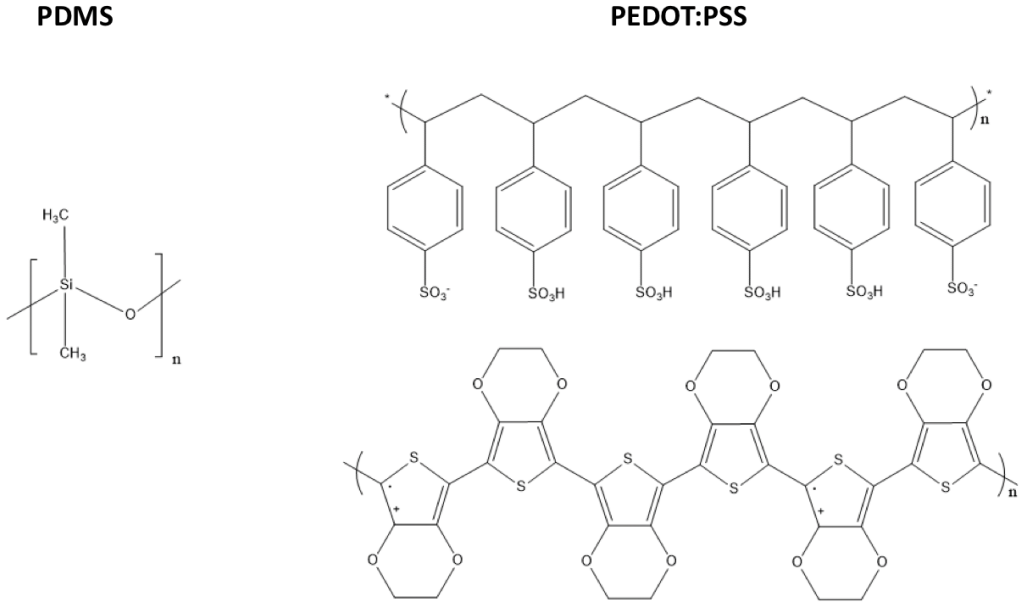

Figure S1. The chemical structures of PDMS and conducting polymer PEDOT:PSS, showing the presence of sulfur element in PEDOT:PSS but not in PDMS.

S2. Origin of sodium content in the PEDOT:PSS/PDMS sponge sensor

The EDX spectrum of the porous PEDOT:PSS/PDMS sponge sensor presented in Figure 2d shows a small peak at around 1.041 KeV, indicating the prescense of sodium content. According to the molecular formulas, there should not be sodium in either PEDOT:PSS or PDMS. To determine the origin of the sodium content, we have spun coated pristine PEDOT:PSS ink onto a silicon wafer and conducted EDX analysis, and observed the same sodium peak (Figure S2). Therefore, we conclude that the sodium content in the PEDOT:PSS/PDMS sponge sensor may be caused by the glassware used during the ink and sample preparation.

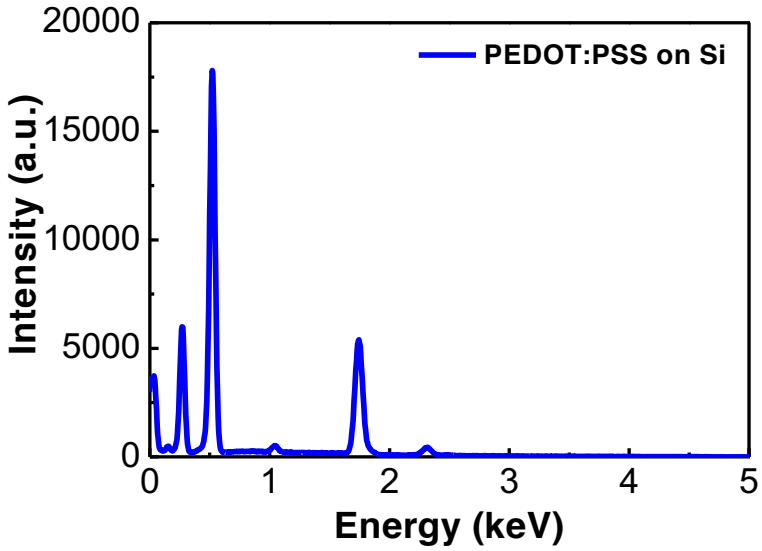

Figure S2. EDX analysis of the PEDOT:PSS thin film spun coated on a silicon wafer.

S3. Mechanical characterization of the porous PEDOT:PSS/PDMS sponge sensor under compressive and tensile strain

The compressive and tensile stress-strain curves were measured by a mechanical testing system (ElectroForce 3200). The PDMS sponge made from brown sugar cubes has a larger micropore size than the one made from white sugar cubes. The mechanical characterization results show that the sponge made from brown sugar cubes with a larger pore size and greater porosity has lower Young's modulus and is thus softer than the sponge made from white sugar cubes with smaller pore size.

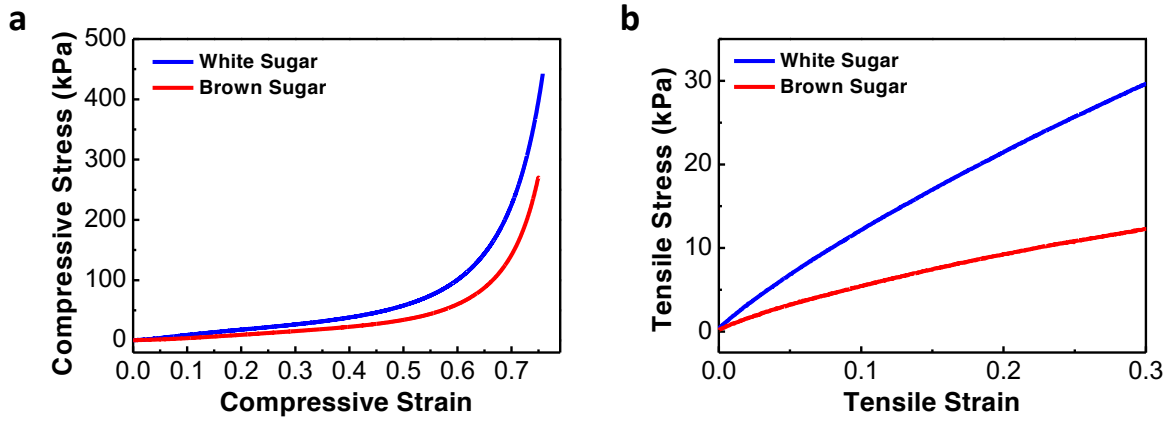

Figure S3. The compressive (a) and tensile (b) stress-strain curves of the porous PEDOT:PSS/PDMS sponge sensor.

S4. Electrical characterization of the porous PEDOT:PSS/PDMS sponge sensor

As shown in Figure S4, the Current-voltage (*I-V*) curves measured from the PEDOT:PSS/PDMS sponge sensors in a relaxed state show a linear relationship. The sensor made from a white sugar cube with a smaller pore size is more resistive than the sensor made from a brown sugar cube.

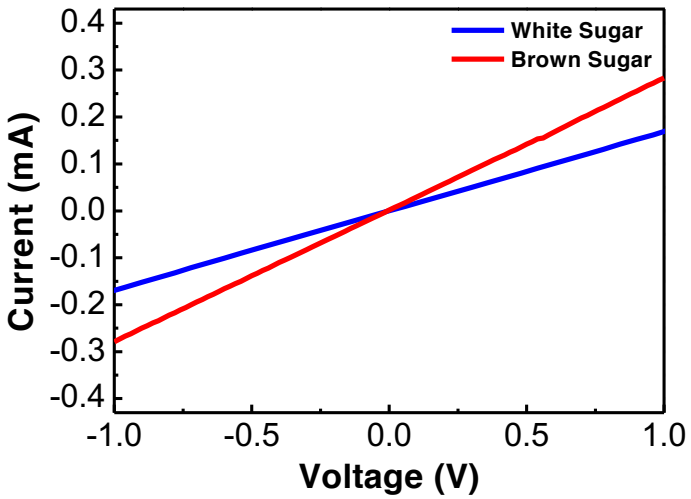

Figure S4. Current-voltage relationship of the porous PEDOT:PSS/PDMS sensors made from white and brown sugar cubes.

S5. Long-term stability of the sensor response to compressive strain

Figure S5 presents the dynamic response of the sensor when a 70% compressive strain was applied and released repeatedly for 1000 cycles. Both the relative change in resistance ($\Delta R/R_0$) and relative change in capacitance ($\Delta C/C_0$) of the sensor remain stable without noticeable change between the 1st – 25th cycle and 975th – 1000th cycle, showing the long-term stability of the sensor response to compressive strain.

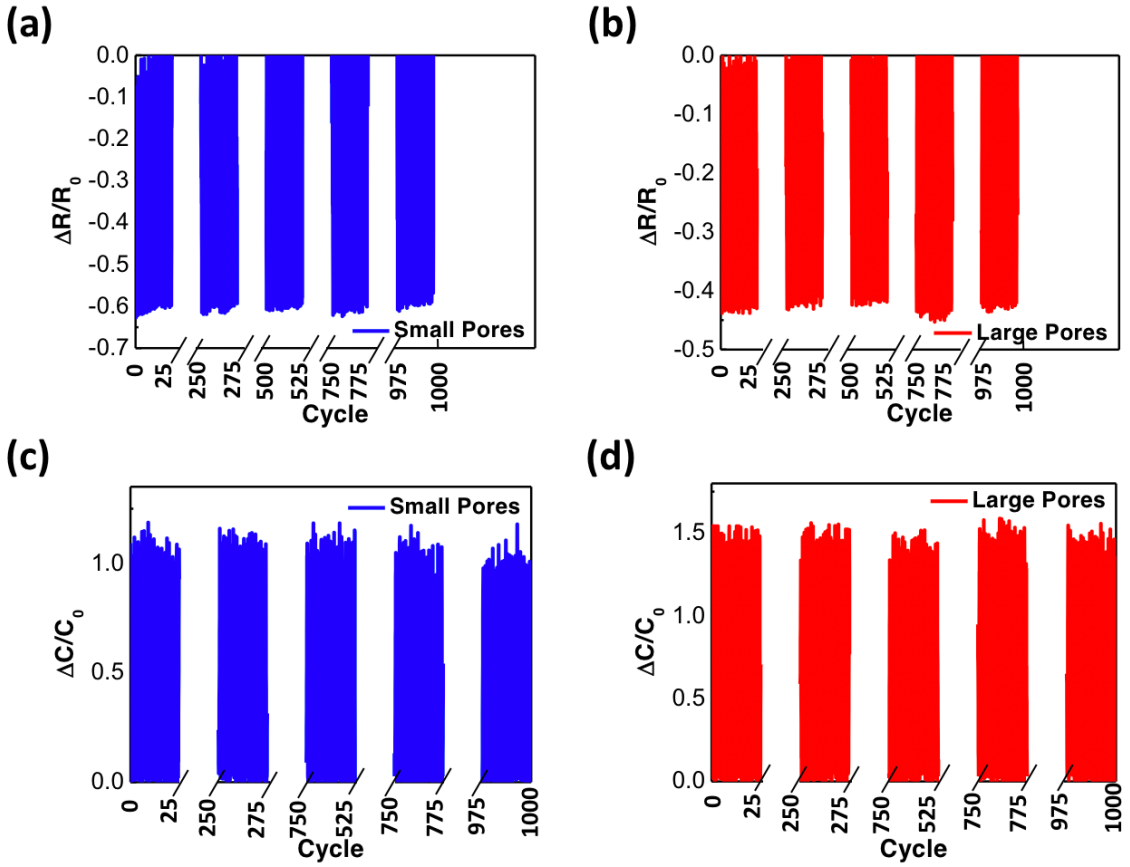

Figure S5. Long-term dynamic response measurements of the porous PEDOT:PSS/PDMS sensor in response to compressive strain. (a, b) Relative change in resistance of the sensor when it was repeatedly compressed to a strain of 70% and released for 1000 cycles. (c, d) Relative change in capacitance of the sensor when it was repeatedly compressed to a strain of 70% and released for 1000 cycles.

S6. Long-term stability of the sensor response to tensile strain

Figure S6 presents the dynamic response of the sensor when it was repeatedly stretched by 30% and released for 1000 cycles. Both the relative change in resistance ($\Delta R/R_0$) and relative change in capacitance ($\Delta C/C_0$) of the sensor remain stable without noticeable change between the 1st – 25th cycle and 975th – 1000th cycle, showing the long-term stability of the sensor response to tensile strain.

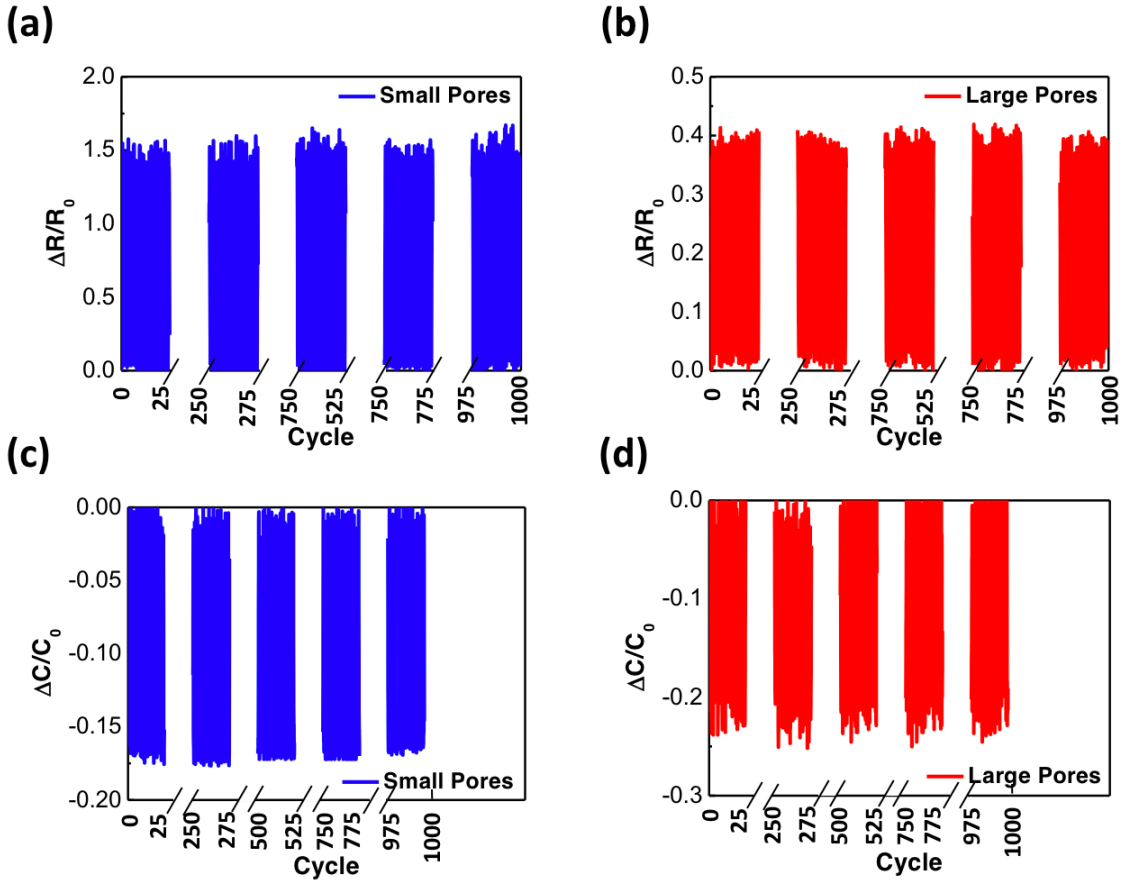

Figure S6. Long-term dynamic response measurements of the porous PEDOT:PSS/PDMS sensor in response to tensile strain. (a, b) Relative change in resistance of the sensor when it was repeatedly stretched to a strain of 30% and released for 1000 cycles. (c, d) Relative change in capacitance of the sensor when it was repeatedly stretched to a strain of 30% and released for 1000 cycles.

S7. Long-term stability of the sensor response to temperature change

Figure S7 presents the relative change in resistance ($\Delta R/R_0$) and relative change in capacitance ($\Delta C/ R_0$) of the porous PEDOT:PSS/PDMS sensor measured at 80 °C during 50 heating/cooling cycles. The sensor was heated to 80 °C on a hotplate when the electrical measurements were taken, and then removed from the hotplate and let it cool down to 20 °C. The heating/cooling cycles were repeated for 50 times. The resistance and capacitance of the sensor measured at 20 °C are defined as R_0 and C_0, respectively. From the results, one can see that the sensor exhibit repeatable response to temperature changes.

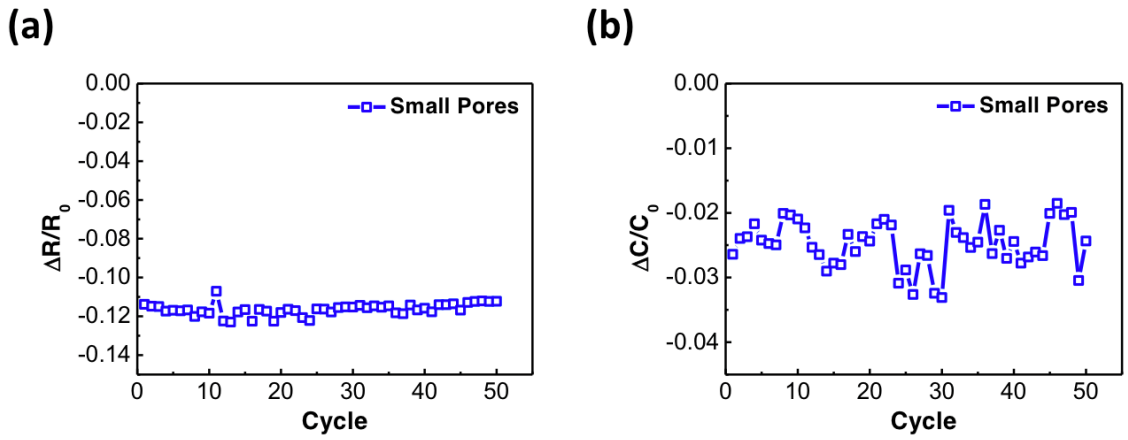

Figure S7. Long-term measurements of the porous PEDOT:PSS/PDMS sensor in response to temperature change. (a) Relative change in resistance of the sensor measured at 80 °C after each heating cooling cycle for 50 cycles. (b) Relative change in capacitance of the sensor measured at 80 °C after each heating cooling cycle for 50 cycles.

Table S1. Comparison of PDMS sponge porosity

The porosity of the porous PDMS sponge is calculated from the equation below. The weight of the porous PDMS sponge was measured on a microbalance, and the PDMS density data were retrieved from the literature.

$$Porosity = \frac{Void\ Volume}{Total\ Volume} = \frac{Total\ Volume - \frac{Weight\ of\ Porous\ PDMS\ Sponge}{PDMS\ Density}}{Total\ Volume}$$

	Porosity	Standard deviation
PDMS sponge made from white sugar cubes	0.6192	0.0145
PDMS sponge made from brown sugar cubes	0.6966	0.0125

Table S1. The porosity comparison between the PDMS sponges made from white sugar cubes and brown sugar cubes.

Table S2. Resistance and capacitance values of the porous PEDOT:PSS/PDMS sponge sensor measured in relax state

	R_0 (Ω)	Standard deviation	C_0 (F)	Standard deviation
Sensor made from white sugar cubes	5955.42	586.87	3.35×10^{-12}	6.17×10^{-13}
Sensor made from brown sugar cubes	2953.90	452.68	3.92×10^{-12}	4.75×10^{-13}

Table S2. Resistance and capacitance values of the porous PEDOT:PSS/PDMS sponge sensor (width, length, and height of the sponge are all 1.5 cm) measured in relax state.

Table S3. Equations for fitting the response curves to different stimuli

Name of the measurement	Pore size	Equation	R^2
$\Delta R/R_0$ vs. Compressive Strain	small	$\Delta R/R_0 = -0.11\cdot\exp(-\varepsilon/-0.52) - 0.11\cdot\exp(-\varepsilon/0.52) + 0.21$	0.9877
$\Delta R/R_0$ vs. Compressive Strain	large	$\Delta R/R_0 = -0.065\cdot\exp(-\varepsilon/-0.197) - 0.065\cdot\exp(-\varepsilon/-0.197) + 0.003$	0.9789
$\Delta C/C_0$ vs. Compressive Strain	small	$\Delta C/C_0 = 0.06\cdot\exp(-\varepsilon/-0.306) + 0.06\cdot\exp(-\varepsilon/-0.306) - 0.137$	0.9950
$\Delta C/C_0$ vs. Compressive Strain	large	$\Delta C/C_0 = 0.38\cdot\exp(-\varepsilon/-0.62) + 0.38\cdot\exp(-\varepsilon/-0.62) - 0.755$	0.9959
$\Delta R/R_0$ vs. Pressure	small	$\Delta R/R_0 = 0.34\cdot\exp(-P/93.15) + 0.344\cdot\exp(-P/93.15) - 0.67$	0.9944
$\Delta R/R_0$ vs. Pressure	large	$\Delta R/R_0 = 0.53\cdot\exp(-P/61.19) + 0.07\cdot\exp(-P/1.9) - 0.58$	0.9908
$\Delta C/C_0$ vs. Pressure	small	$\Delta C/C_0 = -0.8\cdot\exp(-P/178.11) - 0.8\cdot\exp(-P/178.09) + 1.55$	0.9952
$\Delta C/C_0$ vs. Pressure	large	$\Delta C/C_0 = -0.82\cdot\exp(-P/3.71) - 1.07\cdot\exp(-P/57.71) + 1.82$	0.9970
$\Delta R/R_0$ vs. Tensile Strain	small	$\Delta R/R_0 = 0.18\cdot\exp(-\varepsilon/-0.18) + 0.18\cdot\exp(-\varepsilon/-0.18) - 0.38$	0.9697
$\Delta R/R_0$ vs. Tensile Strain	large	$\Delta R/R_0 = 13.73\cdot\exp(-\varepsilon/-18.58) + 13.73\cdot\exp(-\varepsilon/-18.32) - 27.48$	0.9721
$\Delta C/C_0$ vs. Tensile Strain	small	$\Delta C/C_0 = 0.12\cdot\exp(-\varepsilon/0.25) + 0.12\cdot\exp(-\varepsilon/0.25) - 0.24$	0.9923
$\Delta C/C_0$ vs. Tensile Strain	large	$\Delta C/C_0 = 0.13\cdot\exp(-\varepsilon/0.13) + 0.13\cdot\exp(-\varepsilon/0.13) - 0.25$	0.9852
$\Delta R/R_0$ vs. Temperature	small	$\Delta R/R_0 = -1.66\cdot10^{-3}\cdot\cdot T - 1.403\cdot10^{-6}\cdot T^2 + 0.035$	0.9983
$\Delta C/C_0$ vs. Temperature	small	$\Delta C/C_0 = 3.0347\cdot10^{-4}\cdot T - 6.156\cdot10^{-6}\cdot T^2 - 0.0038$	0.9645

Table S3. Summary of fitting curve equations of electrical response to different types of stimuli.

Table S4. Performance comparison of different types of multimodal sensor based on polymer and nanomaterial composites

Materials	Fabrication Method	Sensing Stimuli	Sensitiviy/ Gauge Factor	Sensing Rrange	Repeatability
PDMS/ AgNWs/ CNFs[1]	Dip-coating	Normal pressure	8.21	0-50%	N/A
		In-plane stretch	1.58	0-50%	5000 cycle
		Transverse shear	1.41	0-30%	N/A
PU/CNT[2]	Electrodespinning	Pressure	12.3 N^{-1}	0-5 N	N/A
		Strain	114-720	0-220%	10000 cycle
PTFE/ AgNWs/ Cu/ Graphene/ PDMS[3]	Bar-assisted printing, Dip-coating	Pressure	0.51-15.22 kPa^{-1}	0-40 kPa	N/A
		Temperature	35.2 μV/K	25-60 ℃	N/A
		Materials	N/A	Identify materials	3000 cycle
PU/CB/ AgNWs/ AgNP[4]	Pressure-assisted imprinting/ Dip-coating	Pressure	0.4-32 N^{-1}	0-100 kPa	N/A
		Strain	1041	0-200%	2200 cycle
		Bend	N/A	0-3.5cm (bending radius)	N/A
POMaC/PGS /PLLA/Mg[5]	Thermal evaporate/ Molding	Pressure	0.13-0.7 kPa^{-1}	0-100 kPa	30000 cycle
		Strain	3.33	0-15%	20000 cycle
PDMS/ SWNT[6]	Spray coating	Pressure	0.005-1.5 kPa^{-1}	0-20 kPa	1000 cycle
		Strain	1.16	0-30%	N/A

Supplementary References

(1) Peng, S.; Wu, S.; Yu, Y.; Xia, B.; Lovell, N. H.; Wang, C. H. Multimodal Capacitive and Piezoresistive Sensor for Simultaneous Measurement of Multiple Forces. *ACS Appl. Mater. Interfaces* **2020**, *12*, 22179–22190.

(2) Qi, K.; Zhou, Y.; Ou, K.; Dai, Y.; You, X.; Wang, H.; He, J.; Qin, X.; Wang, R. Weavable and Stretchable Piezoresistive Carbon Nanotubes-Embedded Nanofiber Sensing Yarns for Highly Sensitive and Multimodal Wearable Textile Sensor. *Carbon.* **2020**, *170*, 464–476.

(3) Wang, Y.; Wu, H.; Xu, L.; Zhang, H.; Yang, Y.; Wang, Z. L. Hierarchically Patterned Self-Powered Sensors for Multifunctional Tactile Sensing. *Sci. Adv.* **2020**, *6*, 1–10.

(4) Choi, S.; Yoon, K.; Lee, S.; Lee, H. J.; Lee, J.; Kim, D. W.; Kim, M. S.; Lee, T.; Pang, C. Conductive Hierarchical Hairy Fibers for Highly Sensitive, Stretchable, and Water-Resistant Multimodal Gesture-Distinguishable Sensor, VR Applications. *Adv. Funct. Mater.* **2019**, *29*, 1905808.

(5) Boutry, C. M.; Kaizawa, Y.; Schroeder, B. C.; Chortos, A.; Legrand, A.; Wang, Z.; Chang, J.; Fox, P.; Bao, Z. A Stretchable and Biodegradable Strain and Pressure Sensor for Orthopaedic Application. *Nat. Electron.* **2018**, *1*, 314–321.

(6) Park, S.; Kim, H.; Vosgueritchian, M.; Cheon, S.; Kim, H.; Koo, J. H.; Kim, T. R.; Lee, S.; Schwartz, G.; Chang, H.; Bao, Z. Stretchable Energy-Harvesting Tactile Electronic Skin Capable of Differentiating Multiple Mechanical Stimuli Modes. *Adv. Mater.* **2014**, *26*, 7324–7332.